Composition Limits in Granulation with Active Component in the Binder

David Smrčka, Marek Schöngut, and František Štěpánek
Dept. of Chemical Engineering, Institute of Chemical Technology, Prague, Technicka 5, 166 28 Prague 6, Czech Republic

Tomáš Gregor
New Technologies Research Center, University of West Bohemia, Univerzitni 8, 306 14 Pilsen, Czech Republic

DOI 10.1002/aic.14667
Published online November 11, 2014 in Wiley Online Library (wileyonlinelibrary.com)

The process of reactive granulation is considered. Sodium carbonate primary particles react with dodecyl-benzenesulfonic acid droplets to form granules where the active component is an anionic surfactant formed by the reaction. The effect of primary particle size on the maximum binder/solids ratio was systematically investigated and found to be directly proportional to the specific surface area of the primary particles regardless of how this surface area was achieved—whether by monodisperse powders or bimodal powder mixtures. The effect of binder viscosity on the maximum binder capacity has shown a nontrivial behavior: while the maximum binder content increased with increasing binder viscosity for fine primary particles, the opposite trend was observed in the case of coarse primary particles. This behavior was explained by detailed studies of primary particle wetting and binder penetration into particle beds, as well as by microtomography analysis of the internal granule structure. © 2014 American Institute of Chemical Engineers *AIChE J*, 61: 395–406, 2015
Keywords: granulation, dry neutralization, solid-liquid reaction, powder wetting, reactive wetting

Introduction

The role of a binder in wet granulation is to act as a "glue" that keeps primary particles together initially by capillary forces, eventually solidifying into permanent solid bridges in the final granules.[1–6] In many instances of granulation, the "active" components of the formulation are the primary solid particles, whereas the binder is considered to be only an auxiliary component.[7] This is the case, for example in pharmaceutical granulation, where a mixture of active pharmaceutical ingredient crystals together with other formulation components (excipients) that act as disintegrants, fillers, and so forth, is granulated by means of a relatively small quantity of a liquid, which can be either water or aqueous solution of a polymer.[8,9] In this case, it is usually required to add as little binder as is necessary to achieve the desired granule properties and not to over-granulate the batch.[10–15] However, there are also situations where the active component of the formulation is contained in the binder or formed from the binder by a chemical reaction, while the primary solid particles simultaneously play the role of a reactant and a carrier or structurant. In that case—to maximize the active content of the granules—it is generally desired to add as much binder as possible, while still forming granules rather than a paste.

This is the case of reactive granulation of sodium carbonate primary particles with dodecyl-benzenesulfonic acid (HLAS) as a binder, which is found in the production of detergent powders and is called "dry neutralization" due to the presence of a base in the dry form while the acid is a liquid.[16,17] The chemical reaction between HLAS and sodium carbonate particles yields sodium dodecyl-benzenesulfonate (NaLAS), which is a popular anionic surfactant and is the "active" component of the resulting granules, along with water and CO_2 as reaction by-products. NaLAS forms a solid-like lamellar phase with water, which acts as a "solid" form of the binder and keeps sodium carbonate particles in the granule structure. As the sodium carbonate particles are partially consumed by the reaction but also act as a structurant in the granules, they are used in stoichiometric excess.

The reactive granulation process differs from pharmaceutical granulation not only in the role of the binder but also in the mechanism by which the binder solidifies.[18–20] In pharmaceutical wet granulation, the binder solidifies by drying and the drying usually occurs after granulation,[2,6,7] whereas in the reactive granulation, the binder solidifies as a consequence of a chemical reaction which occurs simultaneously with other elementary steps of granulation, namely binder spreading on primary particles and the nucleation, growth, and coalescence of granules.[21] The outcome of the reactive granulation process, such as the overall conversion, the granule size distribution and porosity, and so forth, is the result of a complex interplay of the chemical reaction with the other elementary steps of granulation.

Correspondence concerning this article should be addressed to F. Štěpánek at frantisek.stepanek@vscht.cz.

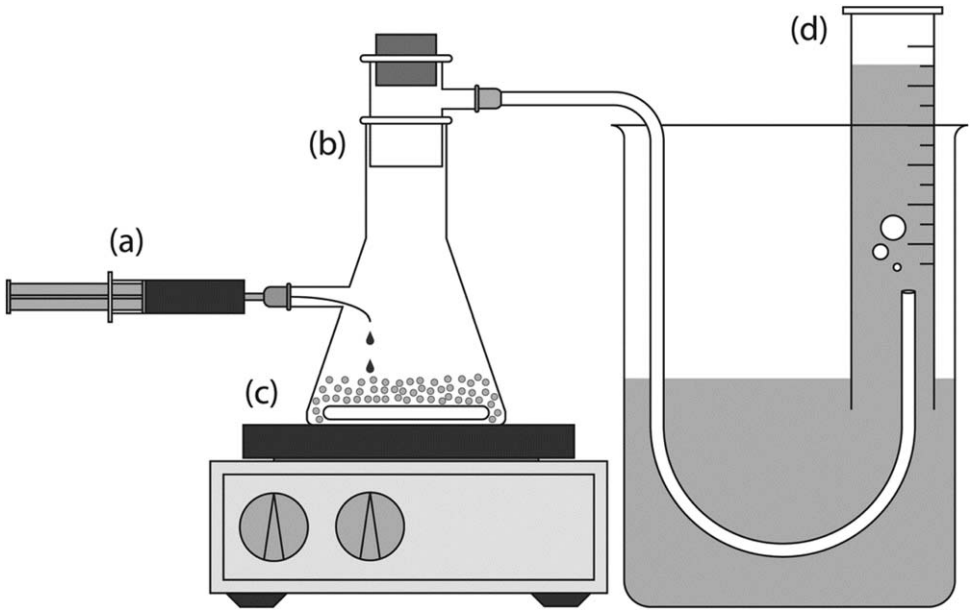

Figure 1. Reaction granulator scheme; (a) medical syringe for drop-wise addition of HLAS, (b) Erlenmeyer flask with magnetic stirrer, (c) heated plate, and (d) graded cylinder for volume measurement.

The kinetics of the dry neutralization reaction was investigated in detail at both local[22] and granulator scale[23] and the influence of various process parameters such as temperature or agitation rate on the progress of both reaction and granulation was subsequently investigated.[24–27] In this work, the aim is to investigate the dependence of the maximum binder/solids ratio in the case of reactive granulation, and to explain the influences of formulation-related parameters such as particles size and binder concentration on the mechanism of granule formation and on the composition limits of granules.

Experimental Methodology

Reactive granulation set-up

The granulation and reaction kinetics measurements were carried out at ambient temperature in an Erlenmeyer flask with agitation provided by a magnetic stirrer. The experimental set-up, shown schematically in Figure 1, was chosen for the sake of consistency with our previous studies and to allow the measurement of reaction kinetics by collecting the CO_2 gas evolved during the neutralization reaction. For each experiment, 20.0 g of sodium carbonate (purchased from Lach-Ner, Czech Republic) was used in the form of narrow size fractions prepared by sieving the raw material using a set of laboratory sieves: 25–56, 56–71, 71–100, 100–140, and 140–180 μm, which will further be denoted S, M, L, XL, and XXL, respectively. The physical properties of the Na_2CO_3 size fractions are summarized in Table 1 and their scanning electron microscopy (SEM) images are shown in Figure 2. During granulation, dodecyl-benzenesulfonic acid (HLAS, purchased from Acros Organics, mixture of C_{10}—C_{13} isomers) was added drop-wise using a medical syringe with a needle diameter of 0.9 mm to maintain a suitable ratio between the flowability of a highly viscous acid and droplet size necessary for sufficient binder distribution to the batch. The added volume was approximately 0.6 mL per run; the exact mass of HLAS added in each experiment was determined by weighing the syringe before and after HLAS addition. The acid addition took between 10 and 15 s.

As CO_2 is a side product of the dry neutralization reaction, a rubber tube was lead from the reaction vessel to a graded cylinder where its volume was recorded as a function of time. Based on earlier experiments, the default stirrer speed was set at 600 rpm to ensure a good binder distribution without breakage or attrition of granules. For the given experimental vessel and stirring speed the Froude number was approximately 0.5, which means that the batch movement is in the transition zone between bumping and roping motion. Unless stated otherwise, the measurements for each set of experimental conditions were carried out three times.

The initial ratio of 0.6 mL HLAS per 20.0 g of Na_2CO_3 results in a large stoichiometric excess of sodium carbonate. To determine the maximum binder/solids ratio that each carbonate size fraction is able to uptake, the additions of binder were repeated until the batch flowability decreased to a point when the stirrer was no longer able to mix the batch. At this stage, the entire batch formed a cake, although individual granules can still be recognized (Figure 3). The amount of added HLAS at this point will be referred to as the

Table 1. Characterization of Prepared Na_2CO_3 Fractions

Powder (-)	Notation (-)	Fraction (μm)	d_{avg} (μm)	a_S ($m^2\ kg^{-1}$)	a_{BET} ($m^2\ kg^{-1}$)	ρ_{bulk} ($kg\ m^{-3}$)	$\rho_{skeletal}$ ($kg\ m^{-3}$)	e_{bulk} (-)
Fine	S	25–56	40.5	58.3	610.1	839.6	2248.8	0.63
Medium	M	56–71	63.5	37.2	897.4	1102.6	2180.3	0.53
Coarse	L	71–100	80.5	29.3	810.4	1164.1	2434.5	0.52
Very coarse	XL	100–140	120.0	19.7	510.4	1238.4	2164.6	0.43
Super coarse	XXL	140–180	160.0	14.8	1219.8	1294.6	2191.4	0.44

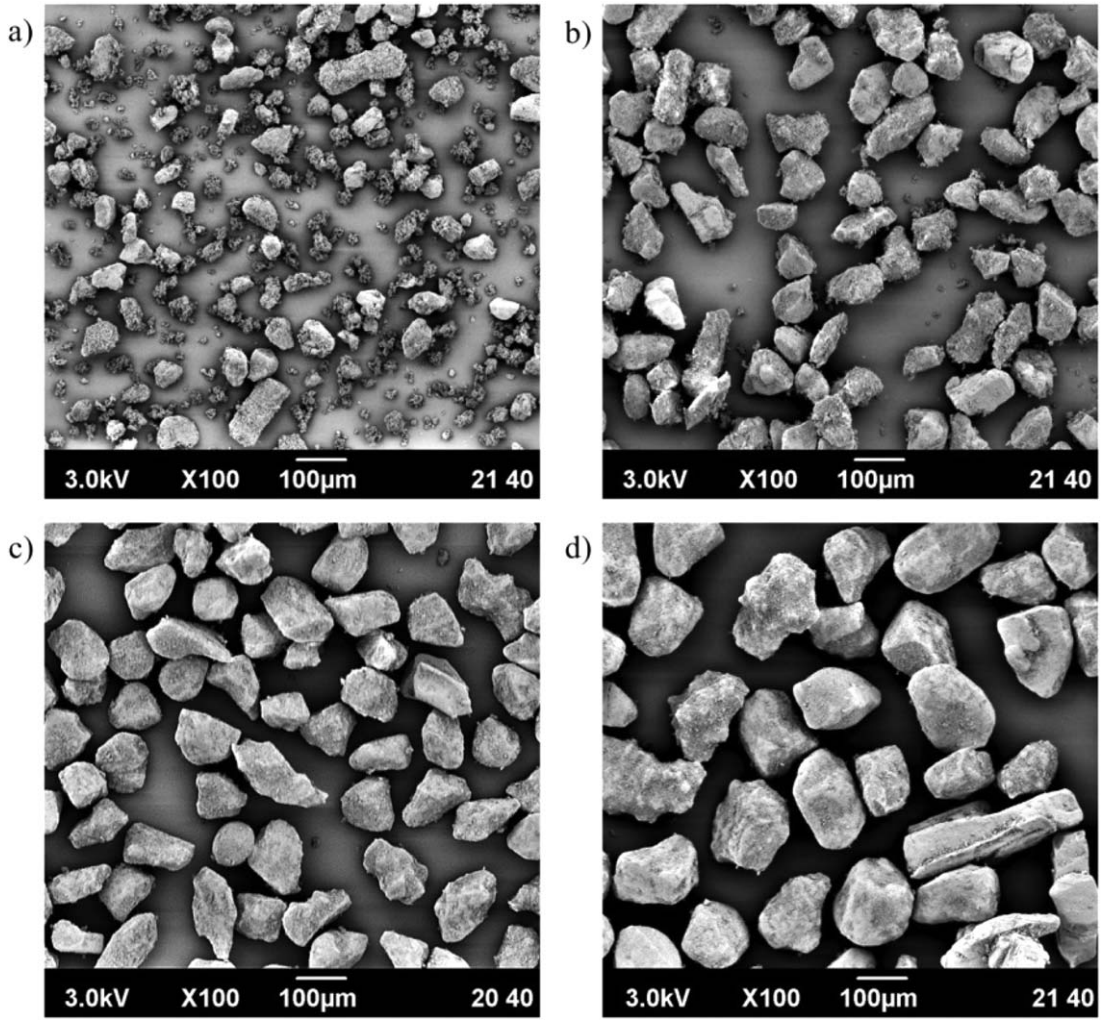

Figure 2. SEM images of sodium carbonate particles of different sizes, used in the experiments: (a) 25–56 μm, (b) 56–71 μm, (c) 71–100 μm, and (d) 100–140 μm.

maximum binder/solids ratio, or L/S_{max}. For the investigation of binder viscosity effects, the HLAS acid was diluted by technical ethanol (denatured by methanol 5 wt %). Five different binder viscosities were used, ranging from 1 mPa s (0% HLAS) to 1700 mPa s (100% HLAS). The full details of binder composition and viscosity are summarized in Table 2.

Particle and binder characterization

The granulated powder was collected after each experiment, spread on a tray and dried at room temperature for 24 h. The size distribution of the whole batch was measured by sieve analysis. The particle morphology was observed using SEM (Jeol JCM-5700). Internal granule structure was investigated by x-ray microtomography (Xradia XCT 400). The dynamic viscosity of the binder solutions was measured using the SV10 vibration viscosimeter (A&D, Japan). The bulk density and porosity of the powder were determined by pycnometry (Micrometrics AccuPyc 1340 and Micrometrics Autopore IV). The total surface area (including internal pores) of the powder was measured by nitrogen sorption (Micrometrics ASAP 2020).

For the characterization of binder penetration into powder beds, several shallow powder beds were prepared in Petri dishes as described in the literature.[28,29] A small droplet of binder was deposited on the powder bed and its evolution in time was recorded at fixed magnification with a Canon EOS 40D camera equipped with a Sigma EX 105 mm macrolens at a rate of 4 frames per second.

Results and Discussion

Effect of primary particle size on the fraction capacity

A basic granulation experiment was carried out by adding approximately 0.6 mL of HLAS into the granulation batch. The volume of evolved CO_2 resulting from each binder addition was recorded and is summarized in Figure 4 for four sieve fractions of sodium carbonate and repeated binder additions until the maximum binder/solids ratio was reached. It can be seen from the figure that although all size fractions initially follow the same trend, the maximum quantity of binder that a batch is able to uptake decreases with increasing primary particle size. Therefore, L/S_{max} was plotted as function of the specific surface area of the primary particles (which was calculated from the particle size assuming spherical particles). As can be seen in Figure 5, there is a very good correlation between L/S_{max} and the calculated specific surface area. The values of L/S_{max} for each size fraction are also summarized in Table 3.

To confirm the trend, additional batches of primary particles were prepared and their L/S_{max} determined. The XXL

Figure 3. Example of a caked batch after achieving L/S_{max}.

[Color figure can be viewed in the online issue, which is available at wileyonlinelibrary.com.]

sieve fraction of Na_2CO_3 (140–180 μm) was measured to extend the range of investigated specific surface areas. In addition, binary mixtures of sieve fractions were prepared so as to reach chosen intermediate values of the specific surface area. The composition of these mixtures is given in Table 4. Note that each binary mixture was prepared in two ways. For example, to obtain a particle mixture with a specific surface area identical to that of the original M fraction (cf. Table 1), particles from the S fraction were mixed either with L or XL particles at different ratios as specified in Table 4. A third type of binary mixture was also prepared which does not correspond to any original fraction. However, its specific surface area falls between those of the S and M fractions. The idea was to cover the range of investigated surface areas more uniformly. As the correlation in Figure 5 demonstrates, the maximum binder/solids ratio is directly proportional to the specific surface area of the powder regardless of how this surface area was achieved.

The process of binder spreading on the primary particles depends on the surface roughness, the bed porosity and the

Table 2. Characterization of Prepared Binder Solutions and Their Maximum Binder/Solids Ratio for Selected Powder Fractions

	c_{HLAS}		L/S_{max} (-)			
η (mPa s)	(mol dm^{-3})	(wt)	S	M	L	XL
1700	3.30	1.00	0.37	0.25	0.17	0.14
947	3.10	0.96	0.30	0.24	0.23	0.18
98	2.60	0.84	0.21	0.24	0.25	0.21
19	2.10	0.69	0.19	0.24	0.25	0.24
1	0.00	0.00	0.18	0.24	0.26	0.24

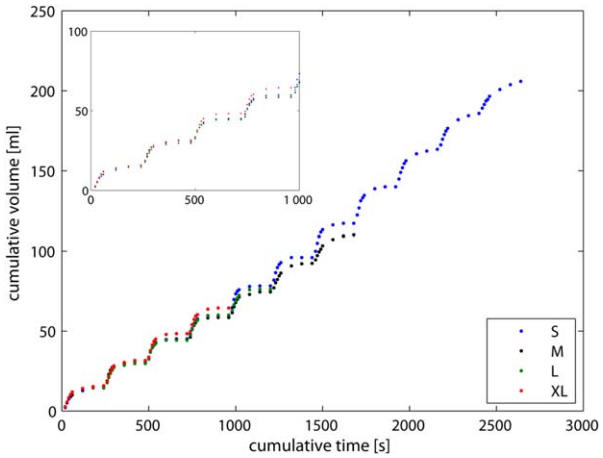

Figure 4. Cumulative volume of evolved CO_2 as function of time for all binder additions until L/S_{max} for each carbonate size fraction (inset: detail of the first 1000 s).

[Color figure can be viewed in the online issue, which is available at wileyonlinelibrary.com.]

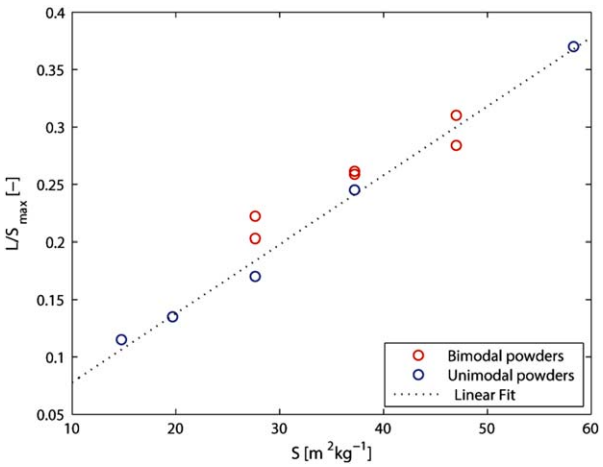

Figure 5. Correlation between L/S_{max} and the calculated specific surface area of primary particles used for granulation.

The composition of the binary powder mixtures is given in Table 4. [Color figure can be viewed in the online issue, which is available at wileyonlinelibrary.com.]

binder viscosity, which changes during reactive granulation as a result of the conversion of HLAS to NaLAS with water as a by-product, and can also be influenced by temperature. Therefore, the next set of experiments was focused on the influence of binder viscosity on the maximum binder/solids ratio.

Table 3. Summary of Reaction Kinetics and Liquid-to-Solid Ratio Results for Selected Powder Fractions

Powder (-)	Notation (-)	Fraction (μm)	N (-)	L/S_{max} (-)	V_{CO2} (mL)	X_{HLAS} (-)
Fine	S	25–56	11	0.37	199.2	72.0
Medium	M	56–71	7	0.25	110.0	60.7
Coarse	L	71–100	5	0.17	76.2	59.3
Very coarse	XL	100–140	4	0.14	64.5	63.0

N is the number of binder additions before reaching L/S_{max}, V_{CO2} is the total volume of evolved CO_2, and X_{HLAS} is the overall conversion of the acid.

Table 4. Composition of Prepared Mixed Primary Powders Given by Weight Fraction and Their Maximum Binder/Solids Ratio

	Composition (-)					
Notation	S	M	L	XL	a_S (m^2 kg^{-1})	L/S_{max} (-)
a	0.465	0.535	–	–	47.0	0.31
b	0.705	–	–	0.295	47.0	0.26
c	0.315	–	0.685	–	37.2	0.26
d	0.455	–	–	0.545	37.2	0.29
e	0.205	–	–	0.795	27.6	0.22
f	–	0.455	–	0.545	27.6	0.21

Effect of binder viscosity on the maximum binder ratio

The dependence of the maximum binder/solids ratio on the binder viscosity is summarized in Figure 6 and Table 2. Depending on the primary particle size, the observed trends are qualitatively different: for the fine particles, L/S_{max} is an increasing function of binder viscosity, for the coarse particles it is a decreasing function, and for the medium size fraction, L/S_{max} is almost independent of the binder viscosity. Moreover, the order of maximum binder/solids ratio at the lowest binder viscosity is reversed compared to that observed for the undiluted HLAS. It is also interesting to note from Figure 6 that for the low-viscosity binder, the L/S_{max} values for the different size fractions are in a much narrower range than in the case of high-viscosity binder.

In general, the trend seen in the case of coarse particles, that is, decreasing L/S_{max} with increasing binder viscosity, is the expected one from the viewpoint of established granulation theory.[28–32] A more viscous binder is generally more effective in binding primary particles together, and so a lower quantity of binder should suffice to fully cake the batch. The opposite trend, seen for the fine particles—where L/S_{max} is 37 % on a mass basis—can be explained by a different mode of binder penetration into the powder bed and a different structure of the wet mass. In the case of fine primary particles and a highly viscous binder, the binder droplet can collect a layer of primary particles on its surface without fully penetrating into the powder bed.

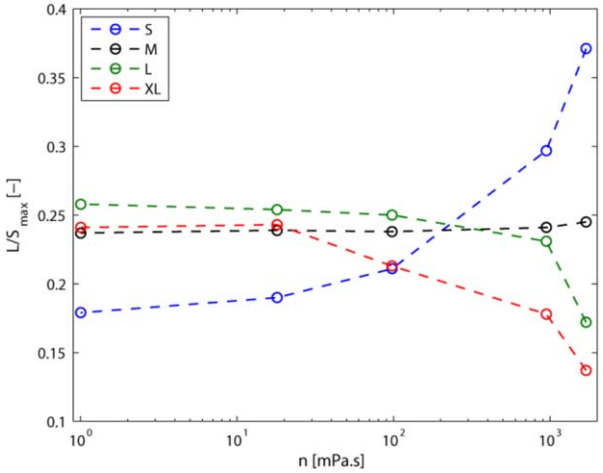

Figure 6. Dependence of L/S_{max} on binder viscosity for each size fraction of primary particles.

[Color figure can be viewed in the online issue, which is available at wileyonlinelibrary.com.]

Reactive binder penetration into powder beds

To confirm this hypothesis, bed penetration experiments[28,29] were carried out using static particle beds consisting of the individual size fractions. Droplets of high-viscosity pure HLAS or lower-viscosity HLAS-ethanol mixture were deposited on the powder bed surface and the evolution of their shape and size was recorded. The outcome of

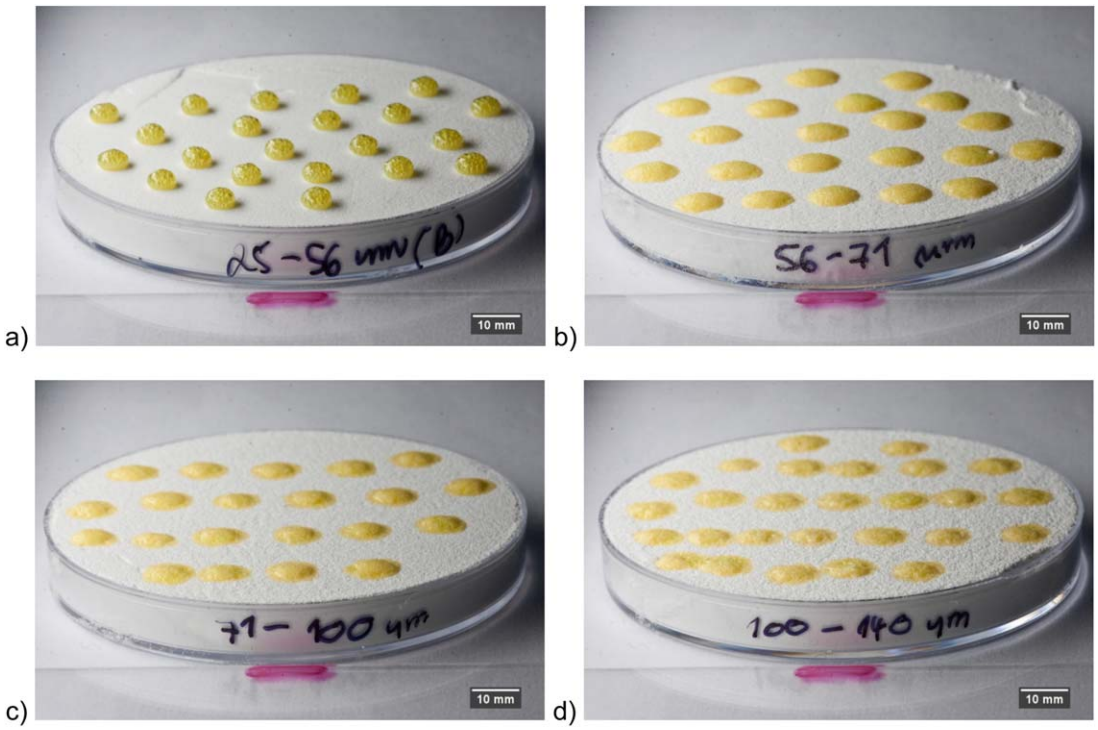

Figure 7. Petri dishes with solidified nuclei after 2 days for different primary particle size fractions as indicated.

[Color figure can be viewed in the online issue, which is available at wileyonlinelibrary.com.]

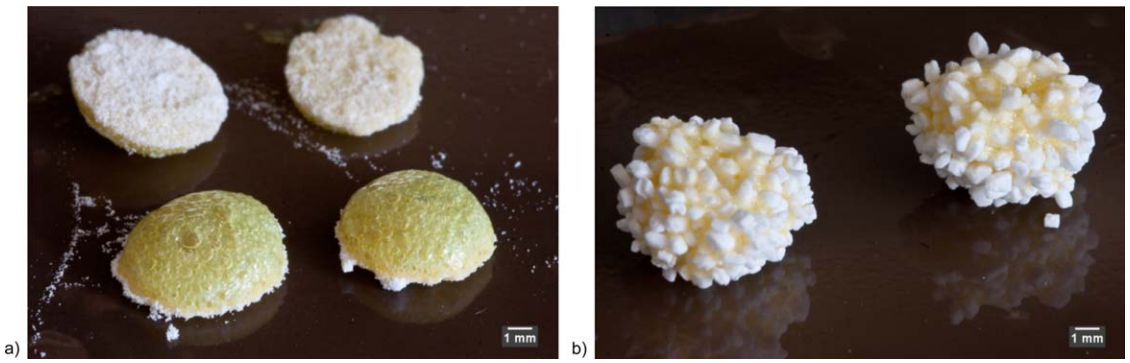

Figure 8. Close up on the solidified nuclei made with (a) very fine Na_2CO_3 powder (0–25 μm) and (b) extreme coarse (500–1000 μm).

[Color figure can be viewed in the online issue, which is available at wileyonlinelibrary.com.]

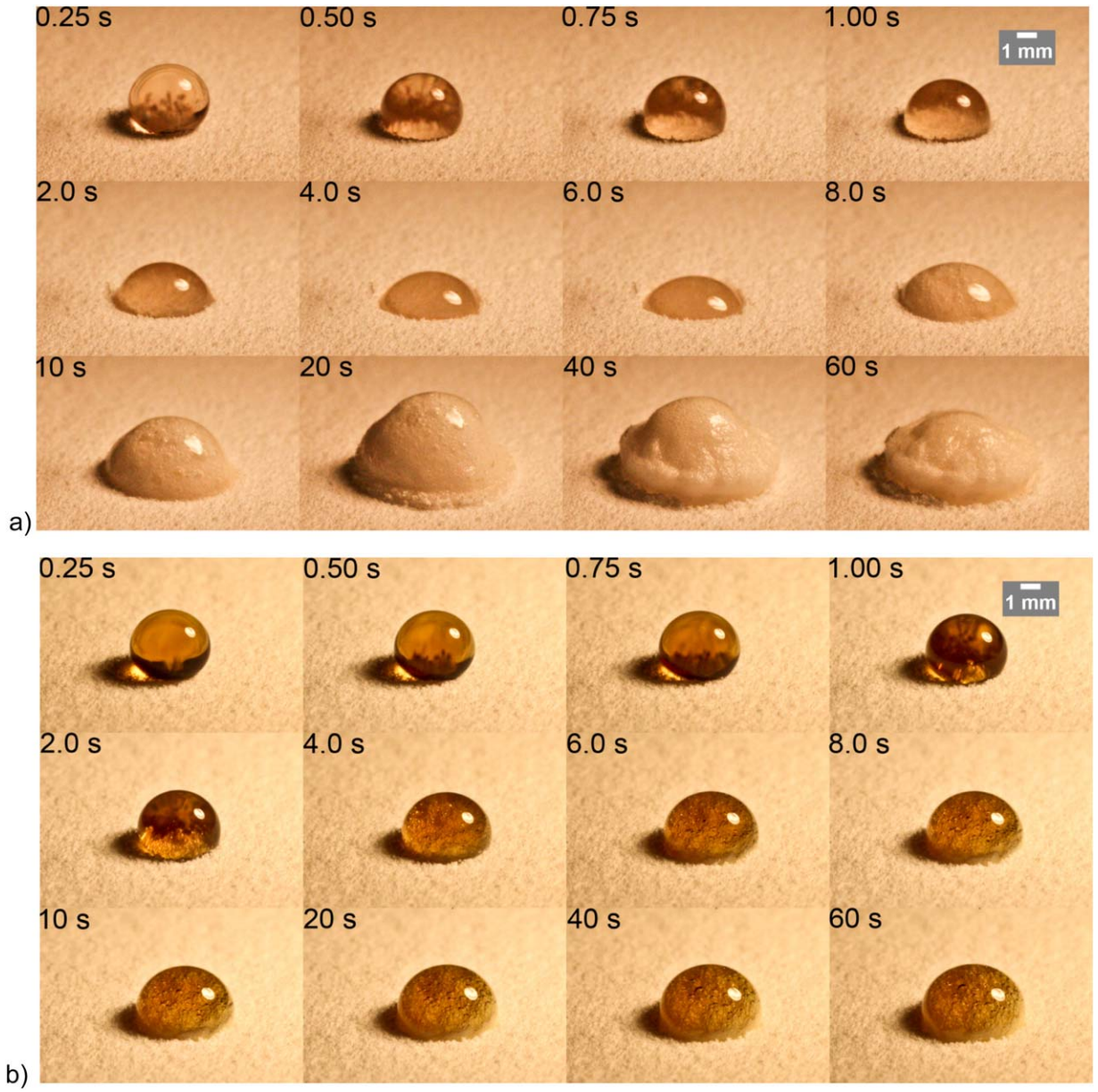

Figure 9. Dynamic evolution of droplet shape for the combinations of two viscosities and two primary particle size fractions.

(a) 19 mPa s and S-particles, (b) 1700 mPa s and S-particles, (c) 19 mPa s and XL-particles, and (d) 1700 mPa s and XL-particles. [Color figure can be viewed in the online issue, which is available at wileyonlinelibrary.com.]

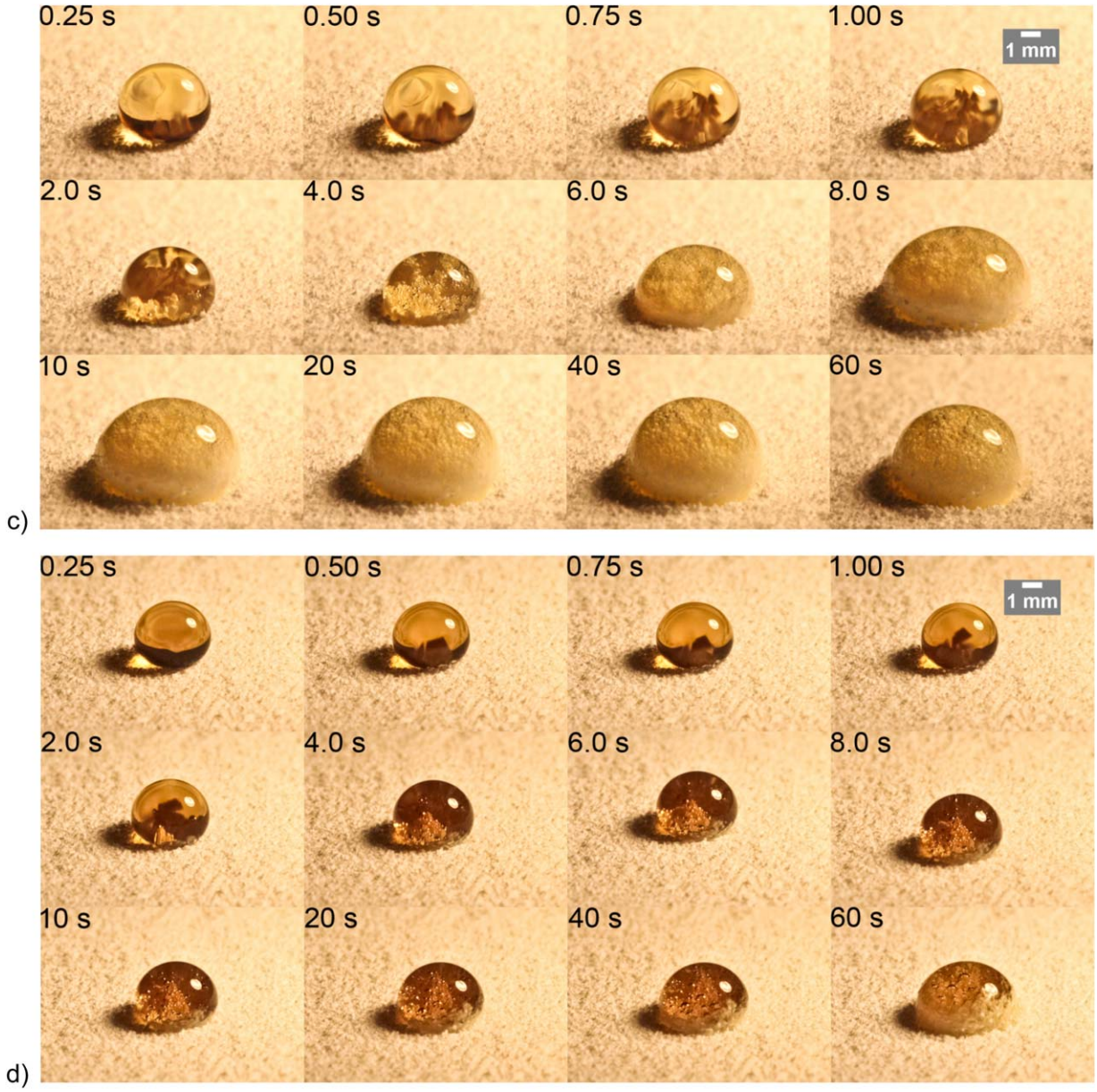

Figure 9. (Continued)

[Color figure can be viewed in the online issue, which is available at wileyonlinelibrary.com.]

the experiment for pure HLAS is shown in Figure 7 for the size fractions S, M, L, and XL. While the acid does not penetrate at all into the bed composed of the fine primary particles, with increasing particle size the extent of penetration improves, ultimately leading to a full immersion of the droplet into the powder bed. This extreme case of full penetration—and the resulting nuclei—is shown in Figure 8.

It should be pointed out that the droplet configurations shown in Figure 7 are asymptotic ones, that is, they no longer evolve in time (the snapshots were taken 2 days after droplet deposition). This is the main difference between the penetration of nonreactive and reactive liquids into a powder bed. While a nonreactive liquid would eventually penetrate into the bed regardless of the particle size, the reactive one forms a solid layer at the liquid-particle interface, which prevents further fluid to be drawn into the powder bed by capillary forces. Thus, the characteristic rate of reaction vs. liquid penetration determines the final outcome. This is shown in Figure 9 where the dynamic evolution of four different cases is compared. In the case of high viscosity (pure HLAS), the droplet remains on the bed surface and the reaction proceeds at the droplet-powder interface at the base of the droplet (Figures 9b,d). Therefore the total liquid-powder contact area is relatively low, although in the case of coarse primary particles (Figure 9d) an interesting phenomenon occurs, namely the spontaneous spreading of primary particles on the droplet surface. Such phenomenon was previously described in the literature in the case of wetting of hydrophobic powders.[33,34] The produced CO_2 bubbles remain in the droplet.

In the case of low viscosity binder combined with fine particles (Figures 9a,c), the characteristic times of droplet penetration and reaction are comparable. The droplet is drawn into the powder bed, increasing the total contact area at which the reaction occurs. As the droplet is partially submerged into the bed (between 4 and 6 s in Figure 9a), the rate of CO_2 evolution overcomes the rate of droplet

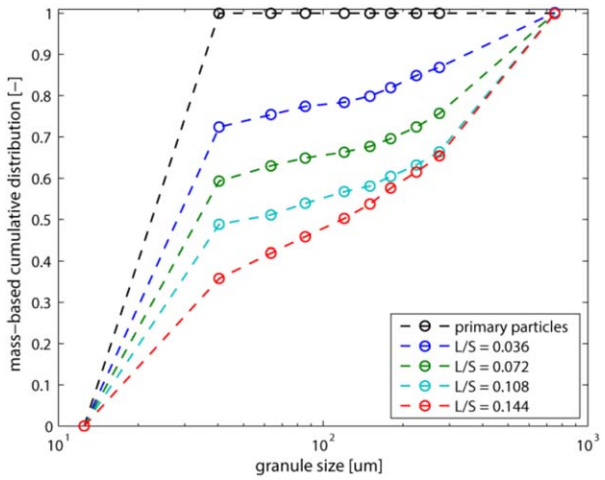

Figure 10. Evolution of granule size distributions with increasing binder/solids ratio for primary particles in the 25–56 μm fraction.

[Color figure can be viewed in the online issue, which is available at wileyonlinelibrary.com.]

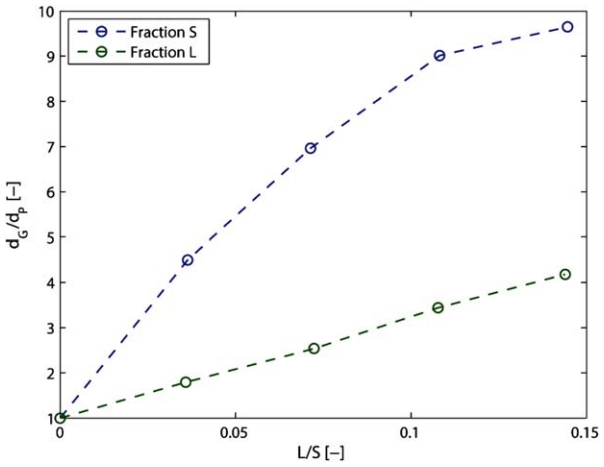

Figure 11. Effect of binder/solids ratio on the relative size of granules within the batch.

[Color figure can be viewed in the online issue, which is available at wileyonlinelibrary.com.]

penetration and the apparent droplet volume starts to increase. Eventually, the apparent droplet volume decreases as some of the CO_2 diffuses out. The extent of shrinkage of the foamed droplet is more significant in the case of the fine primary particles (Figure 9a) than the coarse ones (Figure 9c). However, this phenomenon only occurs for the low-viscosity binder.

Granule size distribution and microstructure

Apart from the maximum quantity of binder that a given size fraction of primary particles is able to uptake, the properties of the final granular product are also of interest. Let us consider the evolution of the size distribution of granules formed from the fine particles with increasing binder ratio, shown in Figure 10 and summarized in Table 5. From the evolving size distribution, it is obvious that further binder additions preferentially cause the removal of ungranulated fines rather than causing coalescence of existing granules. The mode of granule growth can be seen in Figure 11, where the mean granule size is expressed relative to the mean size of the primary particles. The range of binder/solids ratios for which the data are presented in Figure 11 was chosen so as to enable the coarse particles to reach their L/S_{max} (0.14), which is still well below the L/S_{max} of the fine particles (0.37). The mean granule diameter of the coarse particles is approximately four times the primary particle diameter, whereas the mean granule diameter in the case of fine primary particles is nearly 10 times the primary particle size at identical L/S ratio. This is consistent with the idea that granules containing fine primary particles have been formed predominantly by coating of the binder droplet rather than immersion of primary particles into the droplet, a process that can also be seen in Figure 8.

In real industrial granulation, the primary particles are rarely narrow sieve cuts. Therefore, a question arises as to what happens if a binder droplet added to a powder bed has the "choice" of collecting primary particles of different sizes. One possible scenario is that the droplet collects all primary particles indiscriminately in the same proportion in which they are present in the powder bed. An alternative behavior could be that the droplet preferentially collects primary particles of a certain size. If that were the case, then this would have implications for such phenomena as composition nonuniformity or component segregation in multicomponent granulation. To investigate such scenarios, granulation experiments

Table 5. Change of Granule Size Distribution with Increasing Binder/Solids Ratio for the *S* and *L* Size Fractions of Primary Particles

	w_U (wt %)		$w_{<250}$ (wt %)		$w_{>250}$ (wt %)		$d_{4,3}$ (μm)	
L/S (-)	S	L	S	L	S	L	S	L
0.036	72.4	74.1	3.0	13.2	15.3	12.7	126.0	153.2
0.072	59.3	0.5	3.7	62.7	27.6	36.8	194.9	217.0
0.108	48.8	14.2	2.3	50.7	36.9	35.2	252.4	294.1
0.144	35.8	0.5	6.1	48.6	38.4	50.9	270.1	357.3

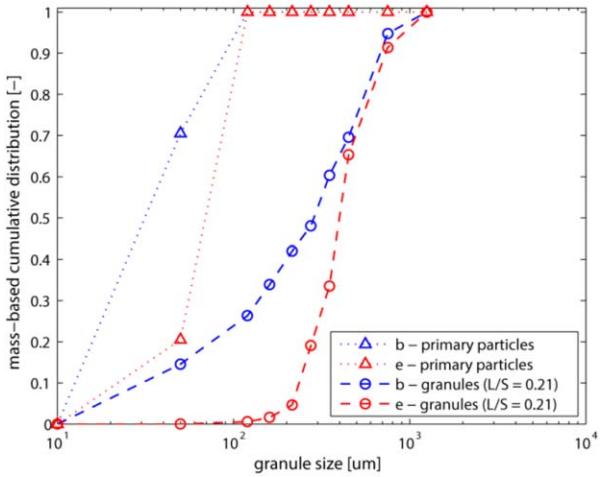

Figure 12. Size distribution of granules formed by the addition of a constant amount of binder into powder beds formed by different binary mixtures of primary particles as indicated in the legend and specified in Table 4.

[Color figure can be viewed in the online issue, which is available at wileyonlinelibrary.com.]

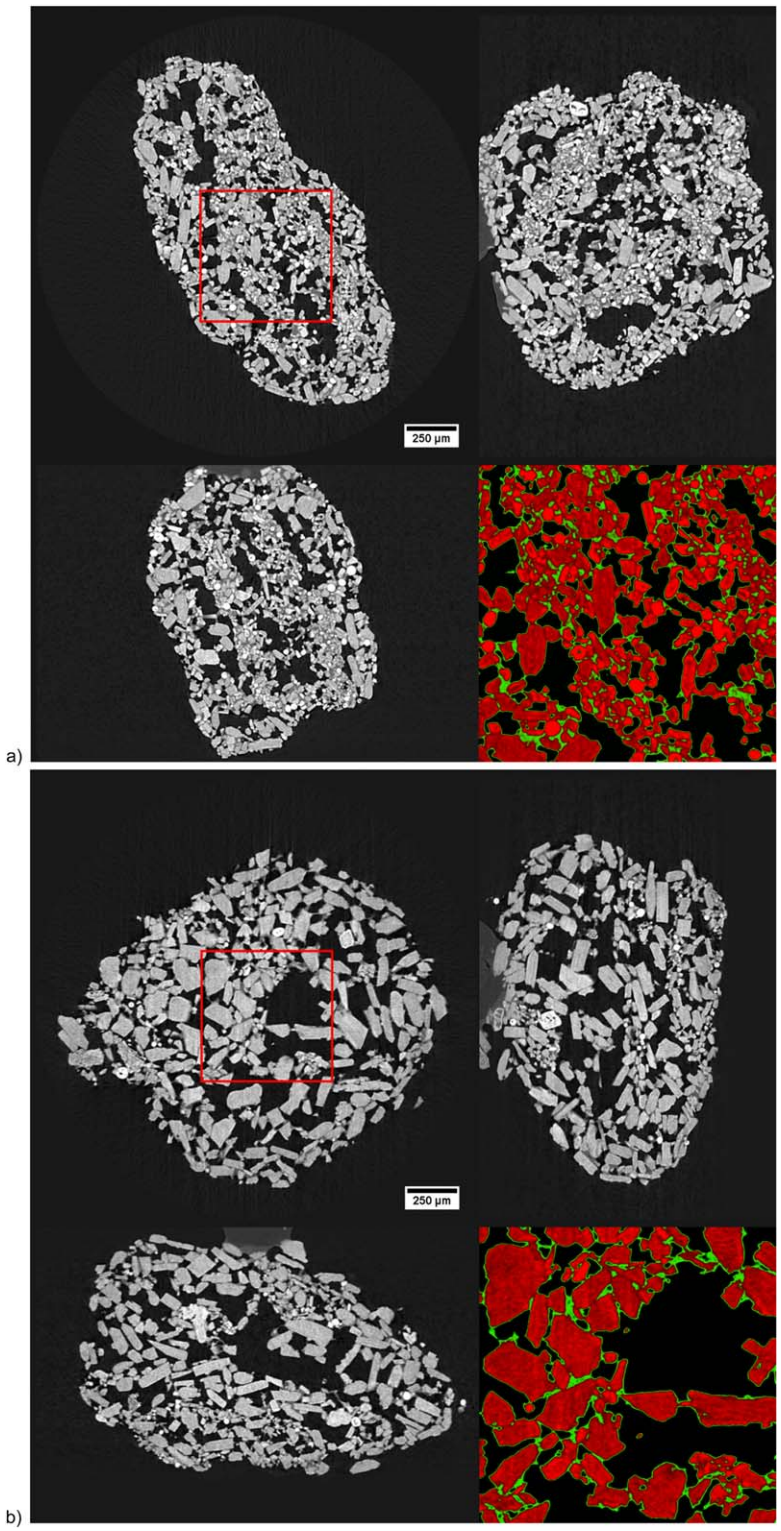

Figure 13. Orthogonal reconstruction of microtomography images; (a) granule from mixed primary powder "b", (b) granule from mixed primary powder "e" (sieve size 500–1000 µm), and (c) granule from mixed primary powder "e" (sieve size 1000–1500 µm).

The inset in each panel contains a magnified section after image segmentation, with primary particles shown in red and binder shown in green. [Color figure can be viewed in the online issue, which is available at wileyonlinelibrary.com.]

were carried out with a constant amount of binder ($L/S = 0.21$) and primary particle batches with a bimodal size distribution obtained by mixing fine (S) and coarse (XL) primary particles at different ratios, namely mixtures denoted as "b" and "e" in Table 4.

The primary particle and granule size distributions obtained from these two mixtures are summarized in Figure 12 and reveal rather different patterns in terms of the mean granule size as well as the fraction of ungranulated primary particles. In the case of mixture "e" (low proportion of fine

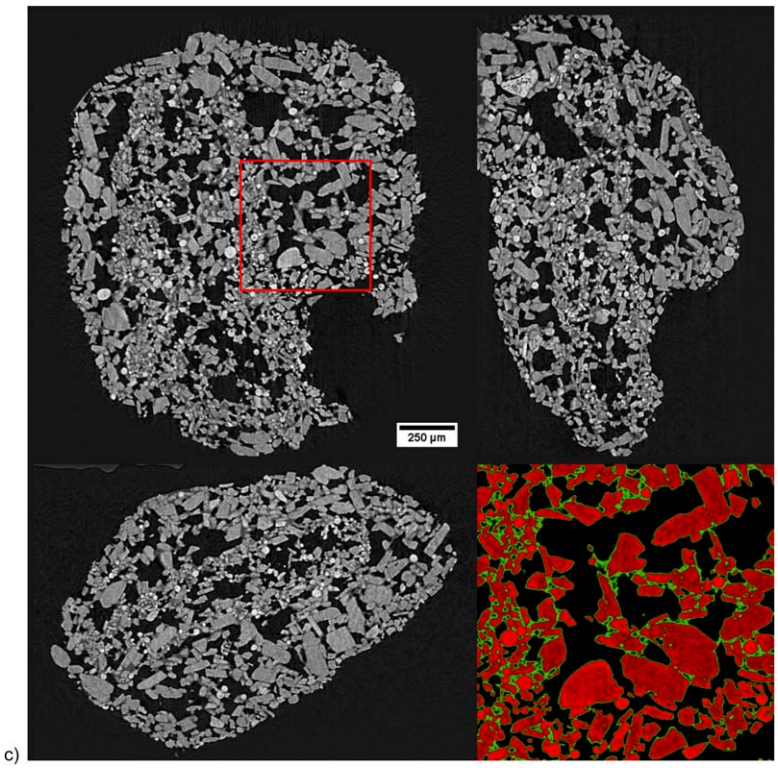

Figure 13. (Continued)

[Color figure can be viewed in the online issue, which is available at wileyonlinelibrary.com.]

primary particles), the fine primary particles are completely consumed during granulation and the resulting granule size distribution is very narrow. Interestingly, also the coarse primary particles have been completely consumed in this case (case "e"), although the relative increase of granule size compared to the size of the coarse part of primary particles is relatively modest (from 120 µm to ~300 µm). In the case of granules resulting from a binary mixture containing a higher proportion of fines (case "b" in Figure 12), there is a remarkable decrease in the proportion of the fine particles, from 0.705 to ~0.15 by weight. This supports the hypothesis of preferential granulation of fine primary particles. It should be noted that the L/S ratio of 0.21, used in Figure 12, is below the L/S_{max} for the fine primary particles, and so one could expect the primary particles to be consumed even further, should more binder be added.

The internal structure of the granules, obtained by x-ray microtomography, is shown in Figure 13. Note that the distribution of fine and coarse primary particles within the granule is not uniform—the fine particles tend to form clusters (often elongated presumably due to shear forces), which also include proportionally higher quantity of binder. The fact that the "local" binder/solids ratio in regions of fine primary particles is higher than that of the granule as a whole is consistent with the previous observation (Figure 4) that fine primary particles are able to uptake a much larger quantity of

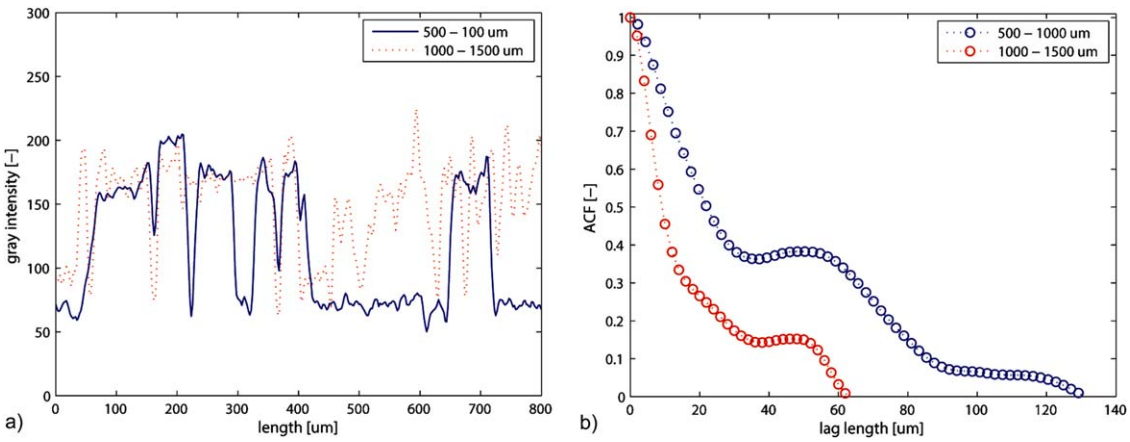

Figure 14. (a) Original intensity-length relationships obtained from the x-ray micro-CT images of two granule size fractions as indicated and (b) autocorrelation functions evaluated form the intensity plots.

[Color figure can be viewed in the online issue, which is available at wileyonlinelibrary.com.]

binder than coarse ones. The coarse particles do not form a wet mass with the binder, they only contain a small quantity of binder at their contact points. Porosity is also distributed nonuniformly. It is present mainly in the form of macropores (or cavities) presumably formed by the evolving CO_2 gas. These macropores are generally not connected to the granule surface, that is, the granule is more compact at its outer perimeter than in its interior.

The microtomography measurements (Figures 13b,c) reveal another interesting phenomenon, namely composition heterogeneity. The granules both originate from the same batch (i.e., case "e" from Table 4) but from different sieve cuts of the final granules: 500–1000 μm in the case of Figure 13b and 1000–1500 μm in the case of Figure 13c. The former granule visibly contains mainly coarse primary particles, while the latter one appears to be composed mainly of fine primary particles. To quantify this visual observation, the autocorrelation functions were evaluated[35,36] from these two images, and are compared in Figure 14. The longer correlation length in the case of the sub-1000 μm granule confirms the presence of coarse primary particles. The possible explanation of such composition heterogeneity is that randomly formed regions of smaller primary particles in the bed are able to carry a larger liquid/solid ratio, which makes it more probable for them to agglomerate into larger granules during subsequent collisions.

Conclusions

The effect of primary particle size on the maximum quantity of binder that a granule can carry has been systematically investigated for a system consisting of reactive primary particle-binder combination, inspired by the reactive granulation used in the manufacture of detergent powders. A linear dependence of the maximum binder/solids ratio (L/S_{max}) on the calculated specific surface area of the primary particles has been found not only for narrow sieve fractions of primary particles, but also for their binary mixtures, and in that case the L/S_{max} did not depend on the exact composition of the mixture, only on its average specific surface. The second investigated parameter was binder viscosity and concentration. It had been observed that the L/S_{max} is a nontrivial function of binder viscosity: for fine primary particles, the maximum binder/solids ratio increases with increasing viscosity, for medium size fractions of primary particles is it flat, and for coarse primary particles the maximum binder/solids ratio is a decreasing function of binder viscosity.

This complex behavior was explained by the interplay between the kinetics of binder penetration into the powder bed (which is faster for lower viscosity and coarser particles), and the kinetics of the chemical reaction between the binder and primary particles (which is faster for more concentrated binder and higher binder-particle contact area). As the reaction product is a solid, which prevents further binder spreading, the final state of the granule can be rather different, which was shown by analyzing the shape of the formed nuclei. Finally, the distribution of fine and coarse primary particles within a granule was investigated by x-ray microtomography and found to be nonuniform across size classes from the same batch. The ability of fine primary particles to attract a higher amount of binder was also observed at the subgranule scale, where regions of high binder content were colocated with the presence of fine primary particles.

Acknowledgments

The authors would like to acknowledge financial support by the Ministry of Education, Youth and Sports (project no. LH12115-MultiGRAN) and by the Specific University Research (MSMT 20/2014). The x-ray tomography facility was funded by the CENTEM project (reg. no. CZ.1.05/2.1.00/03.0088), cofunded by the ERDF as part of the Ministry of Education, Youth and Sports OP RDI program. The authors would like to thank Dr. Lukas Kulaviak for surface area and porosity measurements.

Literature Cited

1. Pietsch W. *Agglomeration Processes: Phenomena, Technologies, Equipment*. Germany: Wiley VCH, 2002.
2. Pietsch W. *Agglomeration in Industry: Occurrence and Applications*. Germany: Wiley VCH, 2004.
3. Litster J, Ennis B. *The Science and Engineering of Granulation Processes (Particle Technology Series)*. The Netherlands: Kluwer Academic Publishers, 2004.
4. Ennis BJ. Theory of granulation: an engineering perspective, In: Parikh DM, editor. *Handbook of Pharmaceutical Granulation*, 3rd ed. New York: Informa Healthcare USA, 2010:6–58.
5. Reynolds GK, Le PK, Nilpawar AM. High shear granulation, in: Salman AD, Hounslow M, Seville JPK, editors. *Handbook of Powder Technology, Vol. 11: Granulation*. Amsterdam: Elsevier, 2006:3–21.
6. Gokhale R, Trivedi NR. Wet granulation in low- and high-shear mixers, In: Parikh DM, editor. *Handbook of Pharmaceutical Granulation*, 3rd ed. New York: Informa Healthcare USA, 2010:183–203.
7. Palzer S. Agglomeration of pharmaceutical, detergent, chemical and food powders—similarities and differences of materials and processes. *Powder Technol*. 2011;201:2–17.
8. Dürig T. Binders in pharmaceutical granulation. In: Parikh DM, editor. *Handbook of Pharmaceutical Granulation*, 3rd ed. New York: Informa Healthcare USA, 2010:78–97.
9. Rowe RC. Polar/non-polar interactions in the granulation of organic substrates with polymer binding agents. *Int J Pharm*. 1989;56:117–124.
10. Staniforth JN, Baichwal AR, Hart JP, Heng PWS. Effect of addition of water on the rheological and mechanical properties of microcrystalline celluloses. *Int J Pharm*. 1988;41:231–236.
11. Sun CC, Himmelspach MW. Reduced tabletability of roller compacted granules as a result of granule size enlargement. *J Pharm Sci*. 2005;95:200–206.
12. Shi L, Feng Y, Sun CC. Roles of granule size in over-granulation during high shear wet granulation. *J Pharm Sci*. 2010;99:3322–3325.
13. Shi L, Feng Y, Sun CC. Origin of profound changes in powder properties during wetting and nucleation stages of high-shear wet granulation of microcrystalline cellulose. *Powder Technol*. 2011;208:663–668
14. Suzuki T, Kikuchi H, Yamamura S, Terada K, Yamamoto Y. The change in characteristics of microcrystalline cellulose during wet granulation using a high-shear mixer. *J Pharm Pharmacol*. 2001;53:609–616.
15. Koide T, Nagato T, Kanou Y, Matsui K, Natsuyama S, Kawanishi T, Hiyama Y. Detection of component segregation in granules manufactured by high shear granulation with over-granulation conditions using near-infrared chemical imaging. *Int J Pharm*. 2013;441:135–145.
16. Smulders E, Rybinsky W, Sung E, Rähse W, Steber J, Wiebel F, Nordskog A. *Laundry Detergents*. Weinheim: Wiley VCH, 2007.
17. Boerefijn R, Dontula PR, Kohlus R. Detergent granulation. In: Salman AD, Hounslow M, Seville JPK, editors. *Handbook of Powder Technology, Vol. 11: Granulation*. Amsterdam: Elsevier, 2006:673–705.
18. Germaná S, Simons S, Bonsall J. Reactive binders in detergent granulation: understanding the relationship between binder phase changes and granule growth under different conditions of relative humidity. *Ind Eng Chem Res*. 2008;47:6450–6458.
19. Germaná S, Simons S, Bonsall J, Carroll B. LAS acid reactive binder: wettability and adhesion behaviour in detergent granulation. *Powder Technol*. 2009;189:385–393.
20. Ramaraji SM, Carroll BJ, Chambers JG, Tiddy GJT. The liquid crystalline phases formed by linear-dodecylbenzene sulphonic acid during neutralization with sodium carbonate. *Colloids Surf A*. 2006;288:77–85.

21. Iveson SM, Litster JD, Hapgood K, Ennis BJ. Nucleation, growth and breakage phenomena in agitated wet granulation processes: a review. *Powder Technol*. 2001;117:3–39.
22. Schöngut M, Grof Z, Štěpánek F. Kinetics of dry neutralization of dodecyl-benzenesulfonic acid with respect to detergent granulation. *Ind Eng Chem Res*. 2011;50:11576–11584.
23. Schöngut M, Smrčka D, Štěpánek F. Experimental and theoretical investigation of the reactive granulation of sodium carbonate with dodecyl-benzenesulfonic acid. *Chem Eng Sci*. 2013;86:2–8.
24. Schöngut M, Smrčka D, Gregor T, Štěpánek F. Investigation of rate-limiting steps during granulation with a chemically reactive binder. *Powder Technol*. 2014; in press, doi:10.1016/j.powtec.2014.05.010.
25. Hibare S, Acharya K. Effect of binder to solid ratio on mechanical properties of granules processed using reactive and non-reactive binder. *Powder Technol*. 2012;229:137–147.
26. Hibare S, Sivanathan R, Nadakatti S. Behaviour of soft granules under compression: effect of reactive and non-reactive nature of the binder on granule properties. *Powder Technol*. 2011;210: 241–247.
27. Hibare S, Acharya K. Scale-up of detergent granules in a high shear mixer. *Powder Technol*. 2014;254:265–273.
28. Clarke A, Blake TD, Carruthers K, Woodward A. Spreading and inhibition of liquid droplets on porous surfaces. *Langmuir*. 2002;18: 2980–2984.
29. Hapgood KP, Litster JD, Biggs SR, Howes T. Drop penetration into porous powder beds. *J Colloid Interface Sci*. 2002;253:353–366.
30. Kumar G, Prabhu KN. Review of non-reactive and reactive wetting of liquids on surfaces. *Adv Colloid Interface Sci*. 2007;133:61–89.
31. Charles-Williams H, Wengeler R, Flore K, Feise H, Hounslow MJ, Salman AD. Granule nucleation and growth: competing drop spreading and infiltration processes. *Powder Technol*. 2011;206:63–71.
32. Rajniak P, Mancinelli C, Chern RT, Štěpánek F, Farber L, Hill BT. Experimental study of wet granulation in fluidized bed: impact of the binder properties on the granule morphology. *Int J Pharm*. 2007; 334:92–102.
33. Charles-Williams H, Wengeler R, Flore K, Feise H, Hounslow MJ, Salman AD. Granulation behaviour of increasingly hydrophobic mixtures. *Powder Technol*. 2013;238:64–76.
34. Hapgood KP, Khanmohammadi B. Granulation of hydrophobic powders. *Powder Technol*. 2009;189:253–262.
35. Štěpánek F, Rajniak P, Mancinelli C, Chern RT, Ramachandran R. Distribution and accessibility of binder in wet granules. *Powder Technol*. 2009;189:376–384.
36. Rahmanian N, Ghadiri M, Jia X, Štěpánek F. Characterisation of granule structure and strength made in a high shear granulator. *Powder Technol*. 2009;192:184–194.

Manuscript received July 22, 2014, and revision received Oct. 8, 2014.